Atmospheric Pb Deposition since the Industrial Revolution Recorded by Five Swiss Peat Profiles: Enrichment Factors, Fluxes, Isotopic Composition, and Sources

DOMINIK WEISS,[†,⊥] WILLIAM SHOTYK,*,[†]
PETER G. APPLEBY,[‡]
JAN D. KRAMERS,[§] AND
ANDRIY K. CHEBURKIN[‖,#]

Geological Institute, University of Bern, Baltzerstrasse 1, 3012 Bern, Switzerland, Environmental Radiometric Research Center, Department of Mathematical Sciences, University of Liverpool, P.O. Box 147, Liverpool L69 3BX, England, Mineralogical-Petrological Institute, Isotope Geology, University of Bern, Erlachstrasse 9a, 3012 Bern, Switzerland, and Institute of Geological Sciences, Ukrainian Academy of Sciences, Gonhkar St. 55-b, Kiev 54, 252054 Ukraine

Atmospheric Pb deposition since the Industrial Revolution was studied in western, central, and southern Switzerland using five rural peat bogs. Similar temporal patterns were found in western and central Switzerland, with two distinct periods of Pb enrichment relative to the natural background: between 1880 and 1920 with enrichments ranging from 40 to 80 times, and between 1960 and 1980 with enrichments ranging from 80 to 100 times. The fluxes also were generally elevated in those time periods: in western Switzerland between 1.16 and 1.55 μg cm^{-2} y^{-1} during the first period, and in western and central Switzerland between 0.85 and 1.55 μg cm^{-2} y^{-1} during the second period. Between the Industrial Revolution and 1985, nonradiogenic Pb became increasingly important in all five cores because of the replacement of coal by oil after ca. 1920, the use of Australian Pb in industry, and the extensive combustion of leaded gasoline after 1950. The introduction of unleaded gasoline in 1985 had a pronounced effect on the Pb deposition in all five cores. Enrichments dropped sharply (between 2 and 4 times), and the isotopic ratios reverted back toward (but not achieving) natural values. The cores from western and central Switzerland showed very similar isotopic trends throughout the time period studied, implying that these sites were influenced contemporaneously by similar pollution sources and atmospheric pathways. Southern Switzerland revealed a different record with respect to the Pb pollution: it was dominated by a single massive Pb enrichment dated between 1930 and 1950. During this period the Pb enrichment factor reached ~200 times background and the Pb flux was ~27 μg cm^{-2} y^{-1}, more than an order of magnitude higher that at the western and central sites. This core also had significantly different post-1950 changes in the Pb isotope ratios.

Introduction

Past atmospheric Pb deposition in Europe has been assessed using a number of archives such as peat bogs (*1–3*), lake sediments (*4–7*), wood from tree rings (*8*), and herbarium plants (*9*). These studies greatly helped to assess anthropogenic perturbations of the natural biogeochemical cycle of Pb. A recent report showed that the greatest Pb flux in western Switzerland (recorded in A.D. 1979) was 1570 times the natural, background flux; even today, these rates are still enhanced by several hundred times (*10*). To identify the sources and to quantify their relative contributions, Pb isotope ratios are widely used. Anthropogenic Pb in the air, derived from high-temperature industrial processes (e.g., steel and nonferrous metal production), fuel combustion (e.g., leaded gasoline, oil, and coal), and incineration (e.g., municipal solid waste) normally has an isotopic signature distinct from naturally occurring Pb supplied by rock weathering (*11*). Gasoline has been the dominant source of recent atmospheric Pb deposition (*2*, *5*), with Pb isotope ratios far from the preanthropogenic values seen during the middle of the Holocene (*10*).

In Switzerland, past atmospheric Pb deposition was mainly studied using lake sediments (*7*, *12–14*). The significant influence of anthropogenic Pb was rigorously demonstrated in these studies. Yet, quantifying atmospheric Pb deposition has been subjected to critical limitations as lake sediments are influenced by lithogenic inputs from catchment soils and rocks which may dominate the atmospheric input (*15*). Studies exclusively quantifying past atmospheric Pb deposition in Switzerland and Central Europe have only been reported very recently (*1*, *10*, *16*, *17*).

Ombrotrophic peat bogs receive all of their water and nutrients from the atmosphere by dry and wet deposition, and provide no measurable chemical influence by groundwater. These systems have a great potential for recording the chronology and magnitude of past atmospheric deposition of immobile elements such as Pb (*18*). If peat bogs are used as archives, it is, however, important to confirm that all the samples of the core used in the reconstruction are in fact ombrotrophic. Vegetation growing at the surface of a bog alone provides no indication about the thickness, stratigraphy, or trophic status of the underlying peat, and groundwater may dominate metal supply to the deeper sections (*19*). Thus, detailed geochemical studies of the bogs of interest are a prerequisite for atmospheric reconstructions (*18*).

In this study, we examined five peat bogs (i) to reconstruct the spatial and temporal pattern of atmospheric Pb deposition over western, central, and southern Switzerland since the Industrial Revolution (covering approximately the last 150 years), (ii) to quantify Pb enrichments relative to natural background values, (iii) to calculate the associated atmospheric fluxes, and (iv) to identify the dominant sources and assess their relative contributions using Pb isotopes. The ombrotrophic and minerotrophic zones of the peat bogs were

* Corresponding author telephone: +41(31)631 8761; fax: +41(31)631 4843; e-mail: shotyk@geo.unibe.ch.
† Geological Institute, University of Bern.
‡ University of Liverpool.
§ Mineralogical-Petrological Institute, Isotope Geology, University of Bern.
‖ Ukrainian Academy of Sciences.
⊥ Present address: Earth, Atmospheric and Planetary Sciences, Massachusetts Institute of Technology, Cambridge, MA 02139.
Present address: EMMA Analytical Inc., Elmvale, Ontario LOL IPO, Canada.

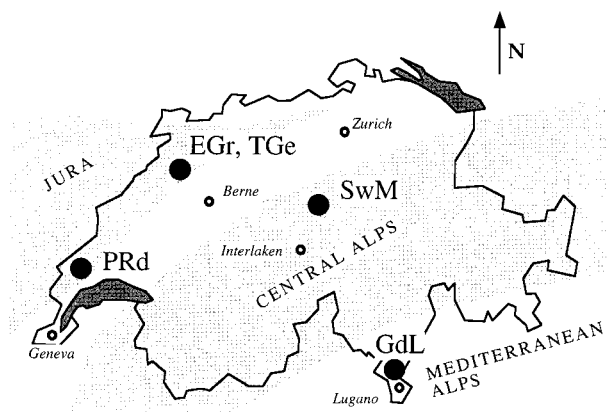| peat core	altitude (m a.s.l.)	mean annual rainfall (mm/y)	coordinates
	Western Switzerland		
Etang de la Gruère (EGr)	1005	1345	570.525/232.150
La Tourbière des Genevez (TGe)	1020	1345	574.000/232.375
Praz Rodez (PRd)	1035	≈1500	502.900/157.900
	Central Switzerland		
Schöpfenwaldmoor (SwM)	1450	≈1900	631.250/177.000
	Southern Switzerland		
Gola di Lago (GdL)	980	≈1800	717.950/106.900

FIGURE 1. Map showing the locations of the five bogs. Three sites (PRd, TGe, and EGr) are located in the Jura Mountains (western part), and two sites (GdL and SwM) in the alpine region (Mediterranean and Central Alps, respectively).

first identified using geochemical indicators, such as ash, Al, and Sr concentrations, and Ca/Mg ratios.

Experimental Section

Site Description. The cores used in this study were collected from peat bogs at Etang de la Gruère (EGr), Tourbière de Genevez (TGe), and Praz Rodet (PRd) in northwestern and western Switzerland (Jura Mountains), at Schöpfenwaldmoor (SwM) in central Switzerland (Central Alps), and at Gola di Lago (GdL) in southern Switzerland (Mediterranean Alps). Figure 1 shows the locations of the sites and Table 1 gives relevant geographical data. All the sites are in rural locations and distant from human settlements, local industry or any other obvious pollution sources.

The uppermost 100 cm at EGr consists of *Sphagnum–Eriophorum* vegetation. At TGe, the uppermost 25 cm are dominated by *Sphagnum–Eriophorum* vegetation and ericaceous shrubs. Remains of sedges (e.g., *Carex*) become increasingly important deeper in the profile, indicating a transition to minerotrophic fen peat. The macrofossil stratigraphies for EGr (20) and TGe (21) are described elsewhere. Geochemical studies of the pore water and solid peat at these two sites were published before (22, 23). PRd and SwM are dominated by *Sphagnum–Eriophorum* vegetation on the top. At SwM, the uppermost 40 cm of the peat core are dominated by *Sphagnum* moss, followed by *Eriophorum* and ericaceous shrubs down to the bottom of the core, implying that this core is ombrotrophic. The macrofossil and pollen stratigraphy of PRd (24) and GdL (25) are described elsewhere. The present day vegetation of GdL consists of typical fen peat vegetation, such as *Trichophorum caespitosum* and *Carex fusca* (18).

Sample Collection and Preparation. With the use of a stainless steel peat profile sampler (26), a 10 × 10 × 100 cm monolith was removed from each of the five peatlands, wrapped in plastic and then aluminum foil, and brought directly to the laboratory. The cores from EGr, TGe, PRd, and GdL were immediately sliced into 3-cm slices using a serrated stainless steel knife. The entire core from SwM was first frozen at −18 °C after collection in the field and then cut while frozen into 1-cm slices using a stainless steel band saw. The peats were dried at 105 °C in Teflon bowls and macerated in a centrifugal mill equipped with a Ti rotor and 0.25-mm sieve. The milling was carried out in a Class 100 laminar flow clean air cabinet to minimize possible contamination from dust.

In the laboratory, all of the sample handling and preparation was carried out using clean laboratory techniques. The cleaning of all the containers and laboratory ware with acids followed previously described procedures (27).

Ash and Major Element Analysis. Al, Mg, and Ca were analyzed by wavelength-dispersive X-ray fluorescence spectroscopy using pressed pellets of dry, solid peat with boric acid added as a supporting matrix. Standardization was accomplished using certified reference materials (22). Ash was determined following the ASTM D 2974 procedure (28). One gram of previously dried, milled, and homogenized peat was dried again at 105 °C. After the sample was cooled in a desiccator, dry weight was determined to 1 mg. Ashing was then accomplished by heating at 550 °C overnight.

Lead and Strontium Analysis. Pb and Sr were measured directly in the dry, solid peat samples using the EMMA miniprobe XRF (29, 30). The minimum detection limit for Pb in solid peat was calculated to be 0.6 μg g^{-1}. The precision of the Pb analyses was ∼30% for concentrations of ∼1 μg g^{-1}, 10% for 10 μg g^{-1}, and 6% for 60 μg g^{-1}. Recoveries for Pb using NBS-SRM 1575 (10.8 μg g^{-1} of Pb) and NBS-SRM 1547 (0.87 μg g^{-1} of Pb) were always within 10% of the certified values. In the core from EGr, Pb was also measured using GFAAS and ICP-MS and the results of the three sets of analyses agreed to within 15% (30).

Scandium Analysis. Five to eight grams of each sample (EGr, TGe, GdL, and PRd) were analyzed using instrumental neutron activation (INAA) for Sc (Activation Laboratories Ltd., Ancaster, Ontario, Canada, (31)). Standard reference materials including coals (NBS-SRM 1632b, NBS-SRM 1635, SARM 19, and SARM 20) and plant materials (NBS-SRM 1575, NBS-SRM 1547, and NBS-SRM 1515, BCR Trace Elements in Rye Grass, IRNAT Lucerne), plus an in-house peat reference material (Ontario Geological Survey OGS 1878P) were analyzed as blind standards in triplicate. Standard deviation, estimated as pooled variances from these measurements, was ± 0.01 μg g^{-1} (22). The detection limit was 0.01 μg g^{-1}.

Lead Isotope Ratios. For the determination of Pb isotope ratios, the peat samples were dissolved using a HNO$_3$/H$_2$O$_2$/HF mixture and microwave heating (32). The isotopes were measured by solid-source thermal ionization mass spectrometry (TIMS) using four Faraday collectors in the static mode (10). Analyses were corrected empirically for fractionation (0.09 ± 0.02% per atomic mass unit) by repeated analysis of the NBS standard 981. The maximum contribution of the procedural blank did not exceed 1.5 ng. This is negligible compared to the total Pb amount in the aliquots (at least 2000 ng in solution). Sample homogeneity was assessed with

triplicate measurements of selected samples from different concentration ranges, and the error was of the same order as the within run standard deviation.

Dating by ^{210}Pb. Dried peat samples from each core were analyzed at the University of Liverpool Environmental Radioactivity Laboratory for ^{210}Pb and ^{226}Ra by direct γ assay, using Ortec HPGe GWL series well-type coaxial low-background intrinsic germanium detectors (*33*). ^{210}Pb was determined via its γ emissions at 46.5 keV, and ^{226}Ra by the 295 and 352 keV γ-rays emitted by its daughter isotope ^{214}Pb following 3 weeks storage in sealed containers to allow radioactive equilibration. The artificial fallout radionuclides ^{137}Cs and ^{241}Am, used to validate the ^{210}Pb results, were measured via their emissions at 662 and 59.5 keV, respectively. The absolute efficiencies of the detectors were determined using calibrated sources and sediment samples of known activity. Corrections were made for the effect of self-absorption of low-energy γ-rays within the sample (*34*).

Results and Discussion

Radiometric Dating by ^{210}Pb. Equilibrium of total ^{210}Pb activity with the supporting ^{226}Ra, corresponding to ~150 years of accumulation, was reached at depths ranging from about 25 cm (Schöpfenwaldmoor) to 62 cm (Praz Rodet). All sites apart from Gola di Lago had similar supported ^{210}Pb (^{226}Ra) activities, with a mean value of 15 ± 1 Bq kg^{-1}. A higher value of 26 Bq kg^{-1} recorded at GdL is due to the much greater concentrations of mineral matter in this core which, in turn, are supplied by surface water flowing through this (minerotrophic) site. At most sites, unsupported ^{210}Pb activity declined nonuniformly with depth, indicating significant variations in the apparent accumulation rate with time. Since mass reduction with time due to organic decay is likely to have been a major contributory factor, ^{210}Pb dates were calculated using the CRS model (*34*). The results of these calculations are given in Table 2. In all cases, the ^{210}Pb dates ca. 1963 are validated by the presence of a significant peak in the ^{241}Am activity versus depth profile, recording the maximum fallout in that year from the atmospheric testing of nuclear weapons (*35*).

The Ombrotrophic vs Minerotrophic Character of the Sites. Figure 2 shows ash, Al, and Sr concentrations and the molar Ca/Mg ratios of each peat core. These geochemical indicators were used to constrain the trophic status of the cores (*18*). Aluminum (conservative element) and ash serve as indicators of the quantity mineral matter supplied to the bog. In ombrotrophic peats, ash concentrations are usually below 5% (*36*). Ca and Sr, both deriving from relatively unstable carbonate minerals, can indicate groundwater influence (by diffusion or mineral matter input) when their concentrations continuously increase with depth, especially in carbonate-rich terrain. Ca/Mg ratios of ombrotrophic peats are expected to be below or similar to regional rainwater (*18, 37*). The molar rainwater ratio used for this study was 6.5, measured at Payerne, a meteorological monitoring site between Bern and EGr (*38*). However, while none of these parameters alone is decisive when trying to distinguish ombrotrophic from minerotrophic peats, taken together with botanical constraints, they provide valuable insight into peatland hydrology and geochemistry.

Ombrotrophic Sites at EGr, PRd, and SwM. The ash concentrations at EGr, PRd, and SwM are generally below 5% throughout the cores except for distinct peaks at 35, 85, and 45 cm, respectively. These correlate with higher peat density (data not shown). Al concentrations are similar in all three cores (up to 0.6%) and correlate strongly with the ash. Both ash and Al are relatively constant with depth, suggesting that no significant additions of mineral matter from the sediment occurred. Also the Sr concentrations are similar at EGr, PRd, and SwM with averages of 7.3 ± 2.1, 10.2 ± 2.2,

and 11.2 ± 2.9 μg g^{-1}, respectively. The profiles are rather constant throughout the core at EGr and PRd. At SwM, Sr concentrations increase slightly with depth (Figure 2), but are still well below the average value in the sediments underlying the bog (41.4 μg g^{-1} at 290 cm). The cores at PRd and EGr have Ca/Mg ratios in general below or similar to the local rainwater ratio of 6.5 (dashed line, Figure 2). The core at SwM has Ca/Mg ratios above local rainwater value below 35 cm. The section used to reconstruct the Pb deposition pattern (top 23 cm), however, is well above that depth.

Minerotrophic Sites at TGe and GdL. At TGe, the molar Ca/Mg ratios below 11 cm are well above the local rainwater values. The continuous increase of the ash, Al, and Sr concentrations and the appearance of sedges such as *Carex* from below 25 cm indicate a transition to minerotrophic fen peat (Figure 2). At GdL, concentrations of Sr (up to 70 μg g^{-1}) and Al (more than 2%) are clearly elevated throughout the profile. Ash concentrations are well above 5% and characteristic of minerogenic peats (*37*). Despite the low Ca/Mg ratios, the very high ash contents obviously indicate significant supply of mineral matter by flowing water. This also agrees with higher supported ^{210}Pb (^{226}Ra) activity and the characteristic fen vegetation.

In summary, the geochemical and botanical variables emphasize strongly that the peat sections used to reconstruct atmospheric Pb deposition are ombrotrophic at EGr, PRd, and SwM and minerotrophic at TGe and GdL.

Lead Concentrations and Pb/Sc Ratios. To correct for natural variations due to differences in ash content or bulk density of the peats, Pb concentrations were normalized to Sc at GdL, EGr, TGe, and PRd and to Al at SwM (Table 2). The rationale and details of the procedure are given elsewhere (*18*). The Pb concentration vs depth profiles in all five bogs differ markedly from each other (Figure 3). Pronounced Pb peaks are distinguishable at EGr (11 and 29 cm, with 86 and 84 μg g^{-1}, respectively) and at SwM (5 and 20 cm, with 70 and 38 μg g^{-1}, respectively). At PRd, concentrations of Pb progressively increase with depth, reaching a maximum of 64 μg g^{-1} at 59 cm. At TGe, a broad peak of 44 μg g^{-1} of Pb is found at 17 cm, and a more pronounced one at 35 cm (59 μg g^{-1}). GdL shows a pronounced peak at 20 cm with 0.15 wt % of Pb, and a much smaller one at 56 cm with 67 μg g^{-1}. However, after normalizing to Sc (EGr, PRd, TGe, GdL) or Al (SwM), each core except GdL has two pronounced peaks: one near the top and a smaller one further down (indicated by arrows in Figure 3). The Pb/Sc peaks occur at 8 and 29 cm at EGr, at 17 and 44 cm at PRd, at 11 and 32 cm at TGe, at 20 cm at GdL. The Pb/Al peaks occur at 8 and 20 cm at SwM. When plotted versus ^{210}Pb age (Figure 3), the Pb/Sc ratios (Pb/Al for SwM) appear contemporaneous. The two peaks at EGr are dated at ca. 1979 and ca. 1905, respectively, at PRd at ca. 1969 and ca. 1913, at TGe at ca. 1975 and ca. 1912, and at SwM at ca. 1964−1971 and ca. 1893. In contrast to these four sites, there is only one peak at GdL at ca. 1945.

Lead Enrichment, Isotopic Composition, and Fluxes. To quantify the atmospheric, anthropogenic Pb enrichments, enrichment factors (EF Pb) were calculated normalizing the Pb/X ratio of individual samples to the natural, background Pb/X ratio (Table 2):

$$\text{EF Pb} = (\text{Pb/X})_{\text{sample}}/(\text{Pb/X})_{\text{background}}$$

where X stands for the conservative, lithogenic elements Sc or Al against which Pb was normalized. The background Pb/Sc ratio of preanthropogenic aerosols was determined in a previous study (*39*) and is 4.1 ± 1.2. In the same set of samples, the average Pb/Al ratio (×1000) is 0.66 ± 0.07 (*n* = 17).

Calculated Pb enrichments against time are shown in Figure 4 for all five peat deposits. The first modern period of significant enrichment lasted from ca. 1880 to 1920 in

TABLE 2. ^{210}Pb Age Dates, Pb, Sc, or Al Concentrations, Pb/Sc or Pb/Al Ratios, Pb Enrichments (EF Pb), and Pb Fluxes (*I*) of the Five Peat Bogs
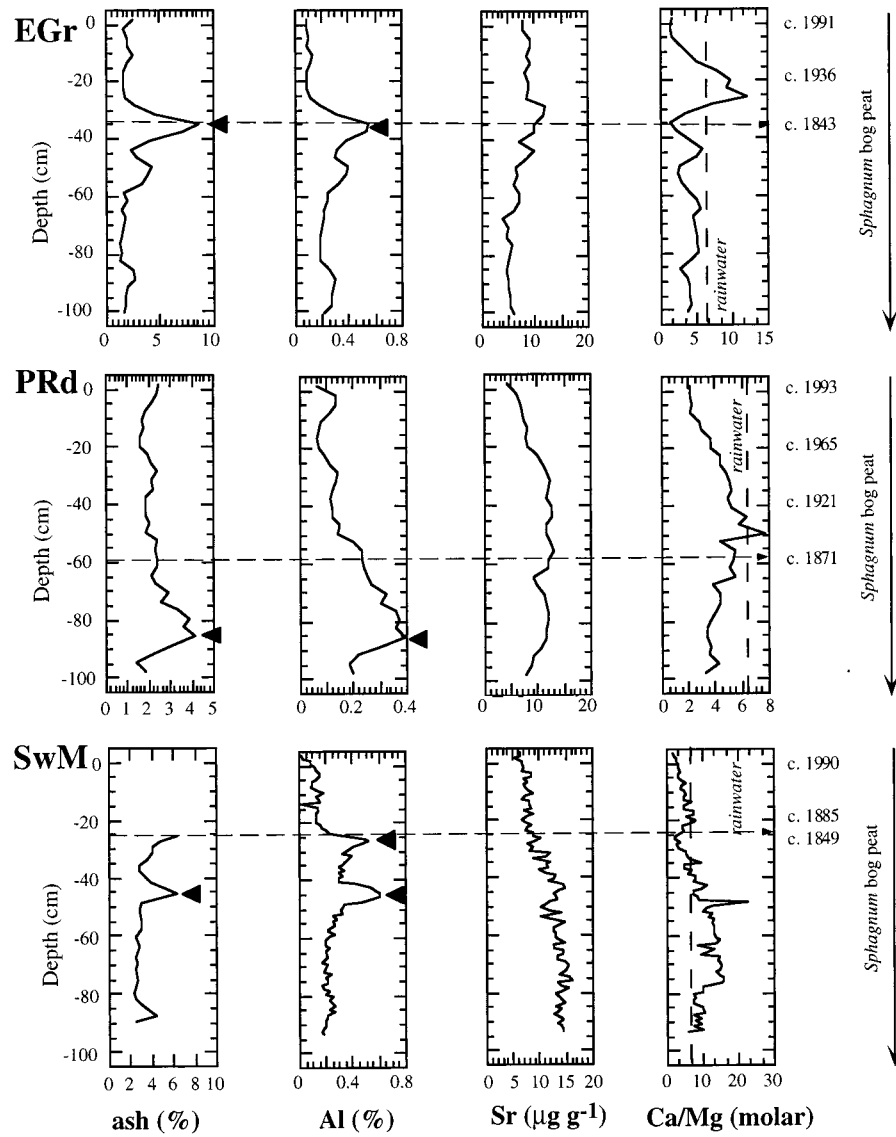
Etang de la Gruère (EGr)

average depth (cm)	age date ^{210}Pb	Pb (µg/g)	Sc (µg/g)	Pb/Sc	EF Pb	*I* (µg cm^{-2} y^{-1})	average depth (cm)	age date ^{210}Pb	Pb (µg/g)	Sc (µg/g)	Pb/Sc	EF Pb	*I* (µg cm^{-2} y^{-1})
1.5	1991 ± 0	14.7	0.12	122.5	29.9		−19.5	1936 ± 3	21.5	0.13	165.4	40.3	0.55
−1.5	1989 ± 2	17.1	0.11	155.5	37.9	0.83	−22.5	1929 ± 3	30.0	0.14	214.3	52.3	0.82
−4.5	1985 ± 2	23.4	0.14	167.1	40.8	0.94	−25.5	1920 ± 4	48.7	0.16	304.4	74.2	1.06
−7.5	**1979 ± 2**	50.5	0.13	388.5	**94.7**	**1.55**	−28.5	**1905 ± 6**	83.9	0.26	322.7	**78.7**	**1.16**
−10.5	1967 ± 2	85.5	0.23	371.7	90.7	1.35	−31.5	1879 ± 11	64.5	0.47	137.2	33.5	0.63
−13.5	1953 ± 2	56.1	0.18	311.7	76.0	0.94	−34.5	1843 ± 25	36.5	0.89	41.0	10.0	0.20
−16.5	1944 ± 2	32.3	0.14	230.7	56.3	0.92							

Praz Rodez (PRd)

average depth (cm)	age date ^{210}Pb	Pb (µg/g)	Sc (µg/g)	Pb/Sc	EF Pb	*I* (µg cm^{-2} y^{-1})	average depth (cm)	age date ^{210}Pb	Pb (µg/g)	Sc (µg/g)	Pb/Sc	EF Pb	*I* (µg cm^{-2} y^{-1})
1.5	1993 ± 0	8.9	0.09	98.9	24.1		−31.5	1943 ± 3	43.3	0.23	188.3	45.9	0.85
−1.5	1990 ± 2	27.1	0.18	150.6	36.7	0.66	−34.5	1936 ± 3	46.3	0.21	220.5	53.8	0.86
−4.5	1985 ± 2	20.3	0.18	112.8	27.5	0.67	−37.5	1929 ± 4	40.5	0.19	213.2	52.0	0.75
−7.5	1981 ± 2	19.9	0.16	124.4	30.3	0.85	−40.5	1921 ± 5	45.1	0.18	250.6	61.1	0.89
−10.5	1977 ± 2	24.2	0.12	201.7	49.2	1.11	−43.5	**1913 ± 6**	47.9	0.19	252.1	**61.5**	0.90
−13.5	1973 ± 2	28.8	0.10	288.0	70.2	1.19	−46.5	1904 ± 7	48.2	0.24	200.8	49.0	0.85
−16.5	**1969 ± 2**	28.9	0.09	321.1	**78.3**	1.11	−49.5	1896 ± 9	52.4	0.23	227.8	55.6	1.03
−19.5	**1965 ± 2**	29.7	0.10	297.0	72.4	**1.20**	−52.5	1888 ± 11	55.3	0.35	158.0	38.5	1.19
−22.5	1961 ± 2	36.6	0.14	261.4	63.8	1.33	−55.5	1880 ± 14	60.5	0.42	144.0	35.1	1.23
−25.5	1956 ± 2	38.2	0.18	212.2	51.8	1.09	−58.5	**1871 ± 17**	64.0	0.40	160.0	39.0	**1.25**
−28.5	1950 ± 2	41.3	0.23	179.6	43.8	0.89							

Schöpfenwaldmoor (SwM)

average depth (cm)	age date ^{210}Pb	Pb (µg/g)	Al (µg/g)	Pb/Al ×1000	EF Pb	*I* (µg cm^{-2} y^{-1})	average depth (cm)	age date ^{210}Pb	Pb (µg/g)	Al (µg/g)	Pb/Al ×1000	EF Pb	*I* (µg cm^{-2} y^{-1})
−0.5	1990 ± 2	39.2	1100	35.6	54.0	0.45	−13.5	1935 ± 3	30.6	1500	20.4	31.2	0.27
−1.5	1987 ± 2	44.1	1300	33.9	51.4	0.46	−14.5	1929 ± 3	29.1	1400	20.8	31.5	0.25
−2.5	1983 ± 2	64.0	1600	40.0	60.6	0.71	−15.5	1923 ± 4	32.9	1400	23.5	35.6	0.26
−3.5	1979 ± 2	57.4	1500	38.3	58.0	0.66	−16.5	1916 ± 4	30.8	1200	25.7	38.9	0.23
−4.5	**1975 ± 2**	69.7	1300	53.6	81.2	**0.85**	−17.5	1909 ± 5	32.3	1300	24.8	37.6	0.21
−5.5	**1971 ± 2**	66.5	1000	66.5	**100.8**	0.80	−18.5	1901 ± 6	34.6	1300	26.6	40.3	0.20
−6.5	**1967 ± 2**	64.3	1000	64.3	**97.4**	0.76	−19.5	**1893 ± 7**	38.4	1300	29.5	**44.8**	0.20
−7.5	**1964 ± 2**	60.3	900	67.0	**101.5**	0.71	−20.5	**1885 ± 9**	36.3	1500	24.2	36.7	**0.27**
−8.5	1960 ± 2	53.6	1400	38.3	58.0	0.71	−21.5	1877 ± 12	32.4	1700	19.1	28.9	0.21
−9.5	1956 ± 2	45.4	1800	25.2	38.2	0.45	−22.5	1868 ± 15	33.8	1900	17.8	27.0	0.21
−10.5	1951 ± 2	43.8	1200	36.5	55.3	0.54	−23.5	1858 ± 18	31.0	2200	14.1	21.3	0.18
−11.5	1946 ± 3	39.6	1400	28.3	42.9	0.36	−24.5	1849 ± 23	30.3	3100	9.8	16.9	0.18
−12.5	1941 ± 3	31.9	1500	21.3	32.2	0.28							

La Tourbière des Genevez (TGe)

average depth (cm)	age date ^{210}Pb	Pb (µg/g)	Sc (µg/g)	Pb/Sc	EF Pb	*I* (µg cm^{-2} y^{-1})	average depth (cm)	age date ^{210}Pb	Pb (µg/g)	Sc (µg/g)	Pb/Sc	EF Pb	*I* (µg cm^{-2} y^{-1})
−1.5	1990 ± 2	15.8	0.12	131.7	32.1	0.69	−22.5	1943 ± 3	40.4	0.18	224.4	54.7	0.95
−4.5	1986 ± 2	28.0	0.17	164.7	40.2	0.93	−25.5	1934 ± 4	37.1	0.23	161.3	39.3	0.76
−7.5	1981 ± 2	34.3	0.19	180.5	44.0	1.17	−28.5	1923 ± 6	41.6	0.23	180.9	44.1	0.85
−10.5	**1975 ± 2**	43.0	0.12	358.3	**87.4**	**1.53**	−31.5	**1912 ± 8**	55.8	0.25	223.2	**54.4**	1.10
−13.5	1967 ± 2	43.0	0.13	330.8	80.7	1.32	−34.5	**1900 ± 11**	58.5	0.27	216.7	52.8	**1.55**
−16.5	1959 ± 2	44.4	0.16	277.5	67.7	1.00	−37.5	1886 ± 15	43.4	0.31	140.0	34.1	0.84
−19.5	1951 ± 3	42.1	0.20	210.5	51.3	1.07							

Gola di Lago (GdL)

average depth (cm)	age date ^{210}Pb	Pb (µg/g)	Sc (µg/g)	Pb/Sc	EF Pb	*I* (µg cm^{-2} y^{-1})	average depth (cm)	age date ^{210}Pb	Pb (µg/g)	Sc (µg/g)	Pb/Sc	EF Pb	*I* (µg cm^{-2} y^{-1})
−1.5	1993 ± 2	127.9	0.32	399.7	97.5	3.7	−19.5	**1945 ± 3**	1527.8	1.80	848.8	**207.0**	**27.7**
−4.5	1987 ± 2	130.3	0.58	224.7	54.8	3.0	−22.5	1932 ± 5	377.2	1.80	209.6	51.1	7.4
−7.5	1979 ± 2	223.0	0.86	259.3	63.2	5.3	−25.5	1915 ± 7	121.8	2.00	60.9	14.9	1.5
−10.5	1972 ± 2	256.1	0.75	341.5	83.3	7.1	−28.5	1894 ± 13	91.3	3.00	30.4	7.4	1.5
−13.5	1964 ± 2	219.8	0.49	448.6	109.4	6.5	−31.5	1876 ± 23	76.8	2.90	26.5	6.5	
−16.5	1955 ± 2	551.6	1.30	424.3	103.5	13.4							

[a] Bold entries indicate peaks in Pb enrichment (PbEF) and fluxes (I) and the corresponding ages.

western (EGr, PRd, TGe) and central (SwM) Switzerland, ranging between 79 (EGr) and 45-fold (SwM). A second period peaked between 1960 and 1980 (Figure 4), with slightly higher Pb enrichments, ranging between 102-fold (SwM) and 78-fold (PRd). While the three peat cores in the Jura Mountains and in central Switzerland have similar Pb-enrichment

Ombrotrophic peat cores

Minerotrophic peat cores

EGr

PRd

SwM

ash (%) Al (%) Sr (μg g⁻¹) Ca/Mg (molar)
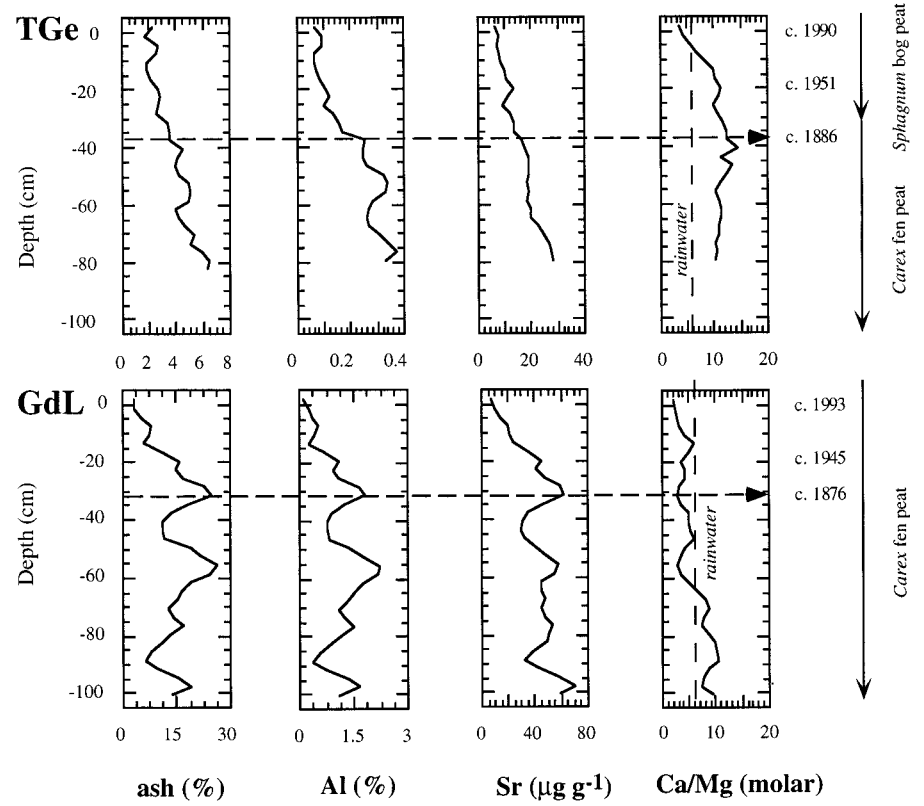
TGe

GdL

ash (%) Al (%) Sr (μg g⁻¹) Ca/Mg (molar)

FIGURE 2. Ash content (%), Al (%) and Sr (μg g⁻¹) concentrations, and the Ca/Mg molar ratio of the peat cores. The dashed line indicates the depth of the oldest ²¹⁰Pb age date. Only those sections which could be age dated using ²¹⁰Pb are discussed in this paper.
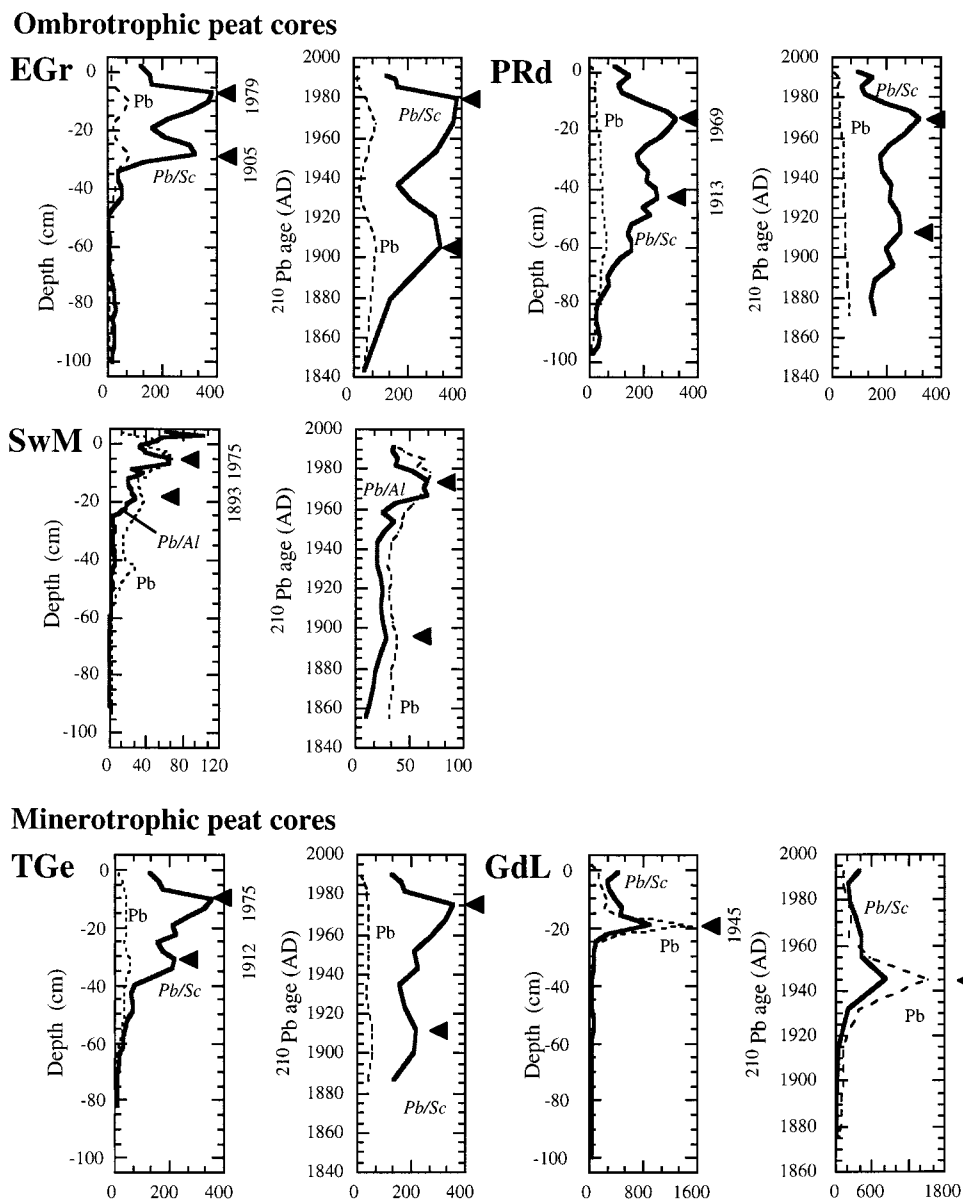
Ombrotrophic peat cores

Minerotrophic peat cores

FIGURE 3. Pb concentrations (μg g^{-1}, dotted line) and Pb/Sc ratios (Pb/Al for SwM, solid line) of the peat cores plotted versus depth and the ^{210}Pb age. The arrows indicate the most pronounced peaks in Pb/Sc (Pb/Al for SwM).

chronologies, the site at GdL displays only one massive Pb enrichment in ca. 1945 (over 200 times background) followed by a strong decrease until the 1980s.

The first period of Pb enrichment in the atmosphere was most likely caused by the increasing industrialization in Europe at the turn of the century (*40*). The use of coal contributed significantly to Pb emissions (*41–43*). Figure 5 shows coal, oil, and gasoline imports to Switzerland (*14*) and the general trends of Pb enrichment in the peat bogs in western and central Switzerland against time. Lead enrichment and coal imports (tons) correlate well during 1843 and 1910 ($r^2 = 0.989$ for EGr, $r^2 = 0.847$ for TGe, $r^2 = 0.931$ for PRd, and $r^2 = 0.706$ for SwM). Lead enrichments at the beginning of the century were also found in Swiss lake sediments of Lake Biel (*14*), Lake Zug (*7*), and Lake Zürich (*13*). The reasons for the decrease around 1920 are most likely stagnating coal imports (Figure 5), the beginning of emission controls (*13*), and the change from coal to heating oil for domestic energy production (*14, 40*). From 1950 on, the Pb enrichment very much follows gasoline imports (Figure 5).

The similarity of the temporal Pb enrichment in the rural peat bogs from different geographic locations in Switzerland north of the main alpine mountain belt (EGr, TGe, PRd, and SwM, Figure 4) indicates mixing of the different emittent sources (industry and traffic) in the atmosphere and transport over large distances before deposition. The temporal Pb-enrichment pattern at GdL differs significantly from the sites north of the main alpine mountain belt (Figure 4), suggesting that the central Alps are an efficient barrier for the transport of pollutant Pb.

Isotopic Composition. The temporal trends of the ^{206}Pb/^{207}Pb isotopic composition are very similar at all five sites (Figure 6, Table 3): constantly decreasing from the mid-19th century until ca. 1945, then an enhanced decrease until the mid-1980s; after this, values increase to more radiogenic ratios. In western and central Switzerland, the ratios are very similar throughout the studied time period. GdL has similar ratios until ca. 1960; afterward, however, they are more radiogenic. To compare the measured trends (denoted as A, B, and C) with the history of Pb used in gasoline in Switzerland, two events are indicated in Figure 6: (i) the

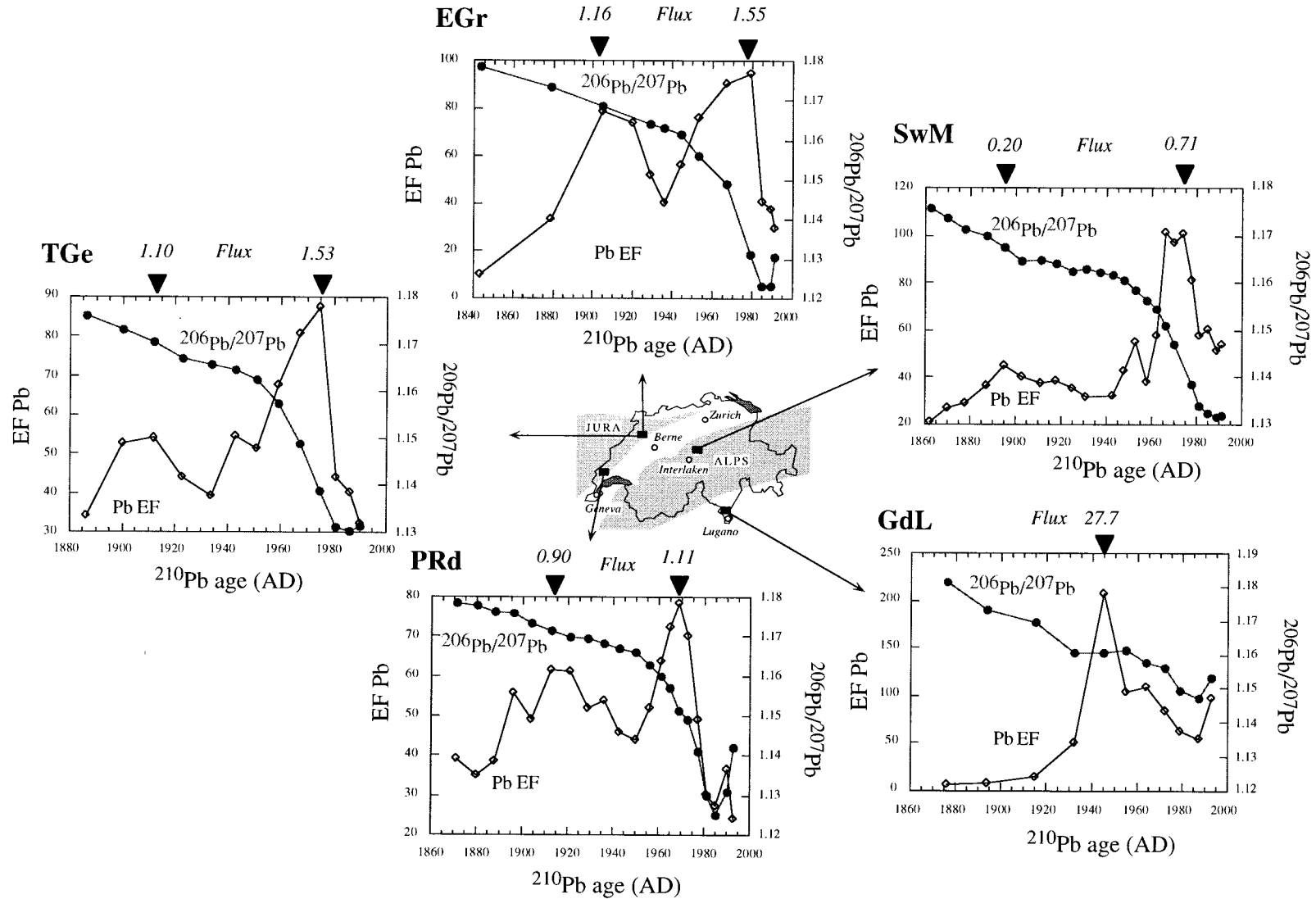**FIGURE 4.** $^{206}Pb/^{207}Pb$ isotope ratios (black dots) and Pb enrichment factors (EF Pb, white diamonds) plotted versus the ^{210}Pb age. Lead enrichments correspond reasonably well with increased Pb fluxes (μg cm^{-2} y^{-1}, shown in italics on top of the graphs). Two distinct periods of Pb enrichment are found in western and central Switzerland.
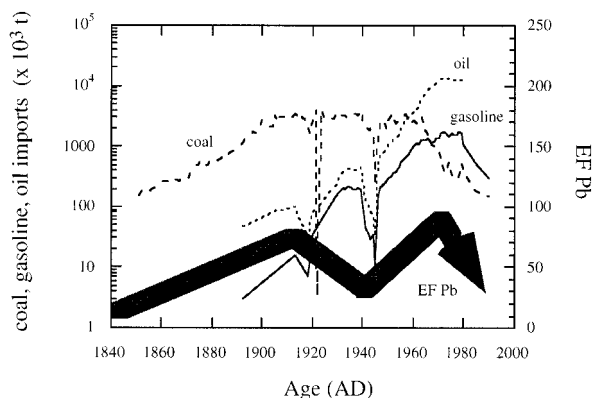
FIGURE 5. Lead enrichment (schematic) of the peat cores at EGr, PRd, TGe, and SwM (broad arrow) and coal, oil, and gasoline imports to Switzerland (taken from ref *14*) during the last 150 years.
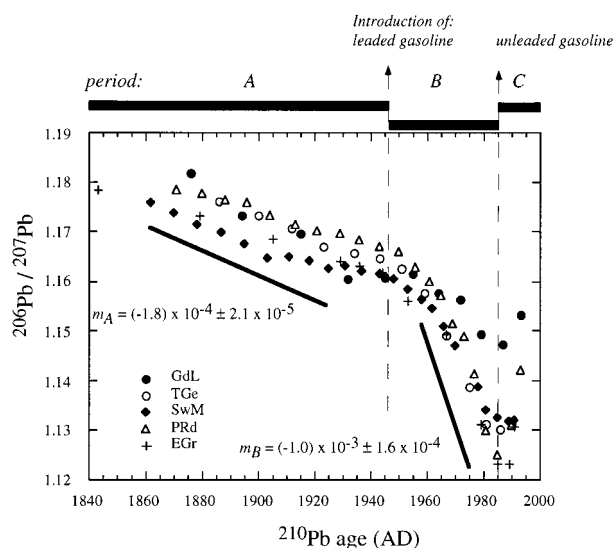

FIGURE 6. $^{206}Pb/^{207}Pb$ isotopic ratios plotted versus ^{210}Pb age of the five peat cores. Three distinct periods A, B, and C are indicated (see text for details). The average slopes m_A and m_B, calculated from the individual slopes of the four peat cores EGr, PRd, TGe, and SwM, are shown for the periods A and B (see Table 4).

introduction of leaded gasoline in 1947 and (ii) the introduction of unleaded gasoline in 1985 (*43*). These two events correspond remarkably well with approximate boundaries between A/B and B/C, respectively. Using these events as boundaries, we calculated the linear regression lines for the periods A and B for each bog (Table 4). Average slopes (m_A and m_B) were calculated from the individual regression lines of each core at EGr, PRd, SwM, and TGe. (GdL was not included in these calculations.) The average slope of B exceeds that of A by 5.6 times and reflects the introduction and growing importance of gasoline Pb (very low $^{206}Pb/^{207}Pb$) on the isotopic composition of atmospheric Pb supplied to the bogs from 1947 to 1985.

Anthropogenic Lead Fluxes at All Five Sites. The anthropogenic Pb flux (I) was calculated from

$$I = [Pb]_a r \quad (\mu g\ cm^{-2}\ y^{-1})$$

where r is the net rate of peat accumulation given directly by the CRS model, using the formula $r = kAC^{-1}$, where k is the ^{210}Pb decay constant, C the ^{210}Pb concentration, and A the cumulative ^{210}Pb. $[Pb]_a$ is the anthropogenic Pb concentration, calculated from
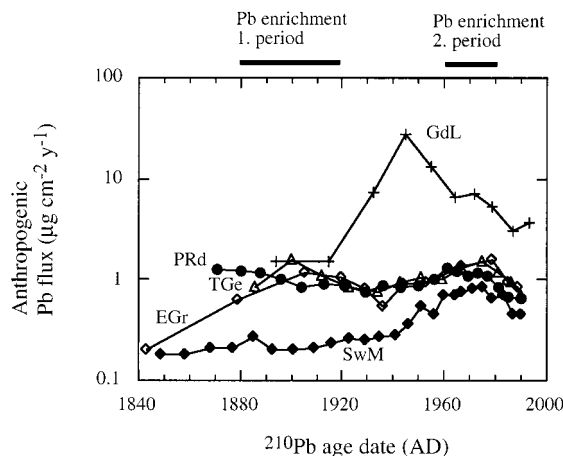
FIGURE 7. Anthropogenic Pb flux ($\mu g\ cm^{-2}\ y^{-1}$) against time of the studied peat cores at SwM (black diamonds), EGr (white diamonds), TGe (white triangles), PRd (black dots), and GdL (crosses). See text for details.

$$[Pb]_a = [Pb] - [X]([Pb]/[X])_{background} \quad (\mu g\ g^{-1})$$

where Pb and X (conservative element) are the measured concentrations in the peat sample. The Pb fluxes versus time (Figure 7) are very similar in western Switzerland (EGr, PRd, and TGe), with peaks of 1.55 $\mu g\ cm^{-2}\ y^{-1}$ in ca. 1900 at TGe and in ca. 1979 at EGr, and agree with the general time vs enrichment pattern. Until recently, Pb fluxes to SwM in the Central Alps were significantly lower than in the western and southern parts of the country, ranging around 0.2 $\mu g\ cm^{-2}\ y^{-1}$ during the Industrial Revolution and with just a small peak in ca. 1885 (0.27 $\mu g\ cm^{-2}\ y^{-1}$). Atmospheric Pb pollution in central Switzerland at that time was probably not as high as in the western part because it is located farther away from the more industrialized countries of France and England. In addition, SwM is at a higher altitude (1450 m a.s.l., Table 1). Since the main pollution source during the turn of the century was coal burning which is associated with large aerosol particles, less Pb appears to have reached SwM at this time compared to the lower altitude sites. High-altitude lake sediments (*12*) and snow layers (*44*) also showed similar changes in Pb deposition during the past century.

Until 1900, the Pb fluxes at GdL were comparable to those in the Jura. Post 1900, however, the fluxes strongly increased and peaked in ca. 1945 with 27 $\mu g\ cm^{-2}\ y^{-1}$. That peak is a pronounced feature which we cannot explain at present. The constant isotopic composition during the time period from ca. 1932 to ca. 1955 (Figure 4) indicates that for more than two decades the same pollution sources were responsible. Elevated concentrations of Cu, Ni, and Zn in these layers (*18*) suggest smelting or other metal processing as the dominant pollution source south of the Alps.

Origin of the Airborne Pb. Three isotope diagrams were plotted to assess in detail the Pb sources and to assign possible mixing end members (Figure 8). Shown are three representative cores: (a) EGr in western Switzerland; (b) SwM in central Switzerland; (c) GdL in southern Switzerland. Included in the diagrams are the isotope ratios (i) from these peat core samples, (ii) from preanthropogenic aerosols (PAA) and average upper continental crust (UCC), (iii) from the main anthropogenic contaminant sources of industry (nonferrous metal production, coal combustion, and waste incineration) and traffic (leaded gasoline), and (iv) from aerosols (measured between 1985 and 1994).

Characterization of Pb Sources. Natural, background Pb is derived from rocks, and its isotopic composition reflects that of the parent material. The Pb isotopic signature of natural aerosols depends therefore on the time integrated

TABLE 3. Isotopic Composition of Pb in the Peat Samples

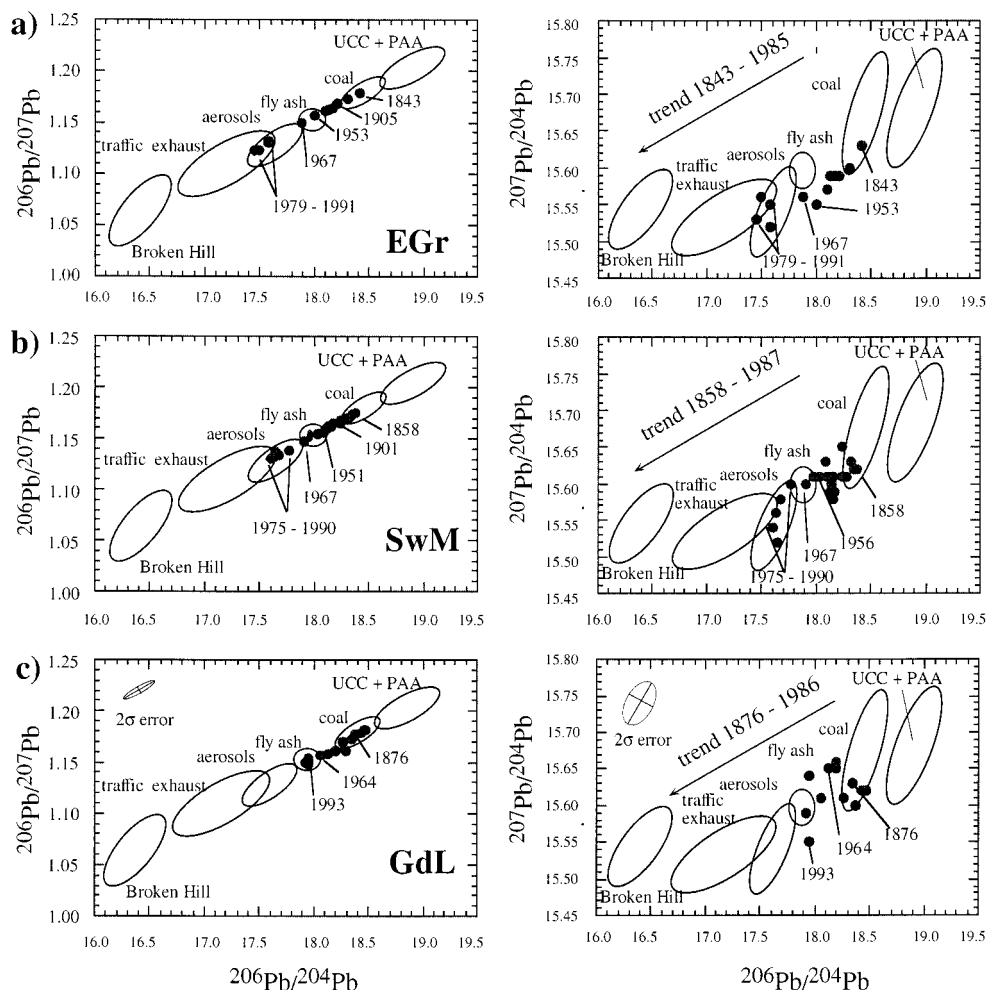| age date ^{210}Pb	206/204	±2σ	207/204	±2σ	208/204	±2σ	208/206	±2σ	206/207	±2σ	age date ^{210}Pb	206/204	±2σ	207/204	±2σ	208/204	±2σ	208/206	±2σ	206/207	±2σ
								Etang de la Gruère (EGr)													
1991 ± 0	17.58	0.03	15.55	0.03	37.37	0.08	2.1242	0.0018	1.1307	0.0004	1944 ± 2	18.10	0.02	15.57	0.02	37.98	0.05	2.0983	0.0005	1.1616	0.0002
1989 ± 2	17.50	0.08	15.56	0.07	37.38	0.18	2.1365	0.0006	1.1232	0.0002	1936 ± 3	18.13	0.02	15.59	0.02	38.01	0.05	2.0972	0.0009	1.1630	0.0023
1985 ± 2	17.46	0.04	15.53	0.04	37.24	0.09	2.1333	0.0005	1.1231	0.0002	1929 ± 3	18.17	0.09	15.59	0.08	38.12	0.19	2.0985	0.0005	1.1641	0.0002
1979 ± 2	17.58	0.04	15.52	0.04	37.37	0.09	2.1260	0.0005	1.1313	0.0002	1905 ± 6	18.22	0.03	15.59	0.03	38.16	0.08	2.0935	0.0017	1.1684	0.0004
1967 ± 2	17.88	0.04	15.56	0.04	37.74	0.02	2.1095	0.0005	1.1492	0.0004	1879 ± 11	18.30	0.03	15.60	0.03	38.24	0.08	2.0892	0.0019	1.1732	0.0005
1953 ± 2	18.00	0.00	15.55	0.01	37.87	0.03	2.1040	0.0005	1.1561	0.0002	1843 ± 25	18.41	0.03	15.63	0.03	38.39	0.08	2.0850	0.0019	1.1784	0.0004
								Praz Rodez (PRd)													
1993 ± 0	17.78	0.02	15.56	0.02	37.53	0.04	2.1105	0.0005	1.1421	0.0002	1943 ± 3	18.24	0.07	15.62	0.06	38.22	0.16	2.0957	0.0009	1.1669	0.0002
1990 ± 2	17.58	0.03	15.53	0.02	37.33	0.06	2.1235	0.0005	1.1310	0.0002	1936 ± 3	18.23	0.05	15.59	0.04	38.18	0.11	2.0937	0.0008	1.1683	0.0002
1985 ± 2	17.48	0.08	15.53	0.07	37.24	0.17	2.1296	0.0005	1.1250	0.0002	1929 ± 4	18.24	0.03	15.58	0.03	38.16	0.06	2.0918	0.0005	1.1695	0.0002
1981 ± 2	17.56	0.02	15.53	0.02	37.33	0.05	2.1256	0.0005	1.1300	0.0002	1921 ± 5	18.27	0.04	15.60	0.03	38.22	0.08	2.0924	0.0006	1.1699	0.0002
1977 ± 2	17.78	0.04	15.57	0.04	37.65	0.09	2.1177	0.0005	1.1412	0.0002	1913 ± 6	18.28	0.03	15.59	0.03	38.20	0.07	2.0904	0.0005	1.1715	0.0002
1973 ± 2	17.87	0.02	15.54	0.02	37.68	0.04	2.1085	0.0005	1.1489	0.0002	1904 ± 7	18.34	0.06	15.62	0.05	38.34	0.15	2.0909	0.0043	1.1733	0.0002
1969 ± 2	17.96	0.06	15.59	0.05	37.87	0.12	2.1086	0.0007	1.1513	0.0002	1896 ± 9	18.35	0.02	15.59	0.02	38.29	0.04	2.0867	0.0005	1.1758	0.0002
1965 ± 2	18.02	0.03	15.56	0.03	37.88	0.07	2.1017	0.0005	1.1570	0.0002	1888 ± 11	18.40	0.03	15.63	0.03	38.44	0.06	2.0889	0.0005	1.1762	0.0002
1961 ± 2	18.12	0.04	15.61	0.04	38.10	0.09	2.1024	0.0005	1.1599	0.0002	1880 ± 14	18.41	0.02	15.62	0.02	38.40	0.05	2.0863	0.0005	1.1777	0.0002
1956 ± 2	18.15	0.05	15.60	0.04	38.08	0.10	2.0979	0.0006	1.1628	0.0002	1871 ± 17	18.41	0.02	15.61	0.02	38.38	0.05	2.0847	0.0005	1.1784	0.0002
1950 ± 2	18.19	0.02	15.58	0..2	38.08	0.04	2.0939	0.0005	1.1660	0.0002											
								Schöpfenwaldmoor (SwM)													
1990 ± 2	17.63	0.03	15.56	0.03	37.45	0.07	2.1247	0.0006	1.1320	0.0002	1935 ± 3	18.14	0.15	15.60	0.13	38.09	0.31	2.0997	0.0005	1.1621	0.0002
1987 ± 2	17.60	0.04	15.54	0.03	37.42	0.08	2.1260	0.0005	1.1316	0.0002	1929 ± 3	18.15	0.06	15.59	0.05	38.09	0.13	2.0992	0.0005	1.1630	0.0002
1983 ± 2	17.64	0.11	15.56	0.10	37.51	0.24	2.1264	0.0005	1.1324	0.0002	1923 ± 4	18.16	0.09	15.61	0.08	38.17	0.19	2.1017	0.0006	1.1625	0.0002
1979 ± 2	17.68	0.04	15.58	0.03	37.61	0.08	2.1268	0.0007	1.1340	0.0002	1916 ± 4	18.15	0.04	15.58	0.04	38.10	0.09	2.0986	0.0005	1.1640	0.0002
1975 ± 2	17.77	0.05	15.60	0.04	37.75	0.10	2.1236	0.0007	1.1386	0.0002	1909 ± 5	18.17	0.05	15.59	0.04	38.13	0.11	2.0984	0.0005	1.1648	0.0002
1967 ± 2	17.91	0.03	15.60	0.03	37.89	0.07	2.1161	0.0005	1.1469	0.0002	1901 ± 6	18.24	0.06	15.65	0.05	38.34	0.13	2.1026	0.0005	1.1646	0.0002
1964 ± 2	17.98	0.06	15.61	0.05	37.98	0.12	2.1127	0.0006	1.1509	0.0002	1893 ± 7	18.24	0.03	15.61	0.03	38.25	0.06	2.0973	0.0005	1.1675	0.0002
1960 ± 2	18.03	0.06	15.61	0.06	38.02	0.14	2.1086	0.0005	1.1546	0.0002	1885 ± 9	18.28	0.07	15.61	0.06	38.29	0.15	2.0949	0.0006	1.1698	0.0002
1956 ± 2	18.08	0.07	15.63	0.06	38.11	0.14	2.1075	0.0005	1.1564	0.0002	1877 ± 12	18.32	0.06	15.63	0.05	38.37	0.13	2.0946	0.0005	1.1713	0.0002
1951 ± 2	18.10	0.06	15.61	0.05	38.10	0.12	2.1046	0.0005	1.1584	0.0002	1868 ± 15	18.35	0.09	15.62	0.08	38.39	0.19	2.0919	0.0005	1.1737	0.0002
1946 ± 3	18.13	0.07	15.61	0.06	38.10	0.14	2.1019	0.0006	1.1605	0.0002	1858 ± 18	18.38	0.18	15.62	0.15	38.38	0.37	2.0886	0.0005	1.1758	0.0002
1941 ± 3	18.13	0.03	15.59	0.03	38.08	0.07	2.1006	0.0005	1.1616	0.0002											
								La Tourbière des Genevez (TGe)													
1990 ± 2	17.58	0.03	15.53	0.02	37.32	0.06	2.1229	0.0005	1.1313	0.0002	1943 ± 3	18.18	0.03	15.61	0.06	38.15	0.05	2.0988	0.0005	1.1647	0.0002
1986 ± 2	17.58	0.03	15.54	0.03	37.39	0.06	2.1263	0.0005	1.1302	0.0002	1934 ± 4	18.18	0.01	15.60	0.02	38.13	0.03	2.0972	0.0005	1.1656	0.0002
1981 ± 2	17.66	0.07	15.62	0.14	37.67	0.13	2.1325	0.0005	1.1311	0.0002	1923 ± 6	18.25	0.02	15.64	0.04	38.31	0.04	2.0998	0.0005	1.1670	0.0002
1975 ± 2	17.74	0.02	15.58	0.04	37.63	0.04	2.1216	0.0005	1.1388	0.0002	1912 ± 8	18.27	0.02	15.61	0.04	38.29	0.04	2.0950	0.0005	1.1705	0.0002
1967 ± 2	17.90	0.02	15.58	0.04	37.80	0.04	2.1124	0.0005	1.1490	0.0002	1900 ± 11	18.31	0.01	15.61	0.02	38.31	0.03	2.0919	0.0005	1.1732	0.0002
1959 ± 2	18.05	0.02	15.59	0.03	38.00	0.03	2.1052	0.0005	1.1575	0.0002	1886 ± 15	18.41	0.02	15.66	0.04	38.49	0.04	2.0903	0.0005	1.1761	0.0002
1951 ± 3	18.13	0.01	15.60	0.02	38.07	0.02	2.0999	0.0005	1.1625	0.0002											
								Gola di Lago (GdL)													
1993 ± 2	17.95	0.04	15.55	0.03	37.74	0.08	2.1028	0.0005	1.1533	0.0002	1945 ± 3	18.19	0.08	15.66	0.07	38.31	0.17	2.1063	0.0008	1.1606	0.0002
1987 ± 2	17.95	0.01	15.64	0.01	37.97	0.03	2.1157	0.0005	1.1472	0.0002	1932 ± 5	18.29	0.18	15.75	0.16	38.62	0.39	2.1116	0.0016	1.1605	0.0002
1979 ± 2	17.92	0.03	15.59	0.03	37.85	0.07	2.1114	0.0007	1.1493	0.0002	1915 ± 7	18.27	0.02	15.61	0.02	38.26	0.05	2.0944	0.0005	1.1696	0.0002
1972 ± 2	18.06	0.04	15.61	0.03	38.05	0.09	2.1061	0.0007	1.1563	0.0002	1894 ± 13	18.35	0.05	15.63	0.04	38.40	0.11	2.0929	0.0005	1.1732	0.0002
1964 ± 2	18.13	0.02	15.65	0.02	38.20	0.05	2.1074	0.0005	1.1576	0.0002	1876 ± 23	18.37	0.01	15.60	0.01	38.33	0.03	2.0867	0.0005	1.1816	0.0002
1955 ± 2	18.19	0.04	15.65	0.03	38.28	0.08	2.1046	0.0005	1.1614	0.0002											

FIGURE 8. Three isotope plots for identification of Pb sources and possible end members. Shown are three peat bogs: (a) EGr (western Switzerland), (b) SwM (central Switzerland), and (c) GdL (southern Switzerland).

TABLE 4. Linear Regression Equations for the Periods A and B

core	period A	period B
EGr	$(-1.7E-04)x+1.49$; $r^2 = 0.999$; $n = 6$	$(-1.1E-03)x+3.22$; $r^2 = 0.973$; $n = 4$
PRd	$(-1.7E-04)x+1.49$; $r^2 = 0.993$; $n = 10$	$(-1.2E-03)x+3.50$; $r^2 = 0.962$; $n = 9$
SwM	$(-1.7E-04)x+1.50$; $r^2 = 0.969$; $n = 12$	$(-0.8E-03)x+2.76$; $r^2 = 0.983$; $n = 9$
TGe	$(-2.1E-04)x+1.57$; $r^2 = 0.990$; $n = 6$	$(-1.1E-03)x+3.25$; $r^2 = 0.992$; $n = 5$
GdL	$(-1.9E-04)x+1.53$; $r^2 = 0.946$; $n = 4$	$(-4.4E-03)x+2.01$; $r^2 = 0.976$; $n = 5$

U/Pb and Th/Pb ratios of their source rocks. In this study, natural background Pb is represented by preanthropogenic aerosols (10) and upper continental crust (45) (^{206}Pb/^{207}Pb 1.19−1.22; ^{206}Pb/^{204}Pb 18.68−19.11; ^{208}Pb/^{204}Pb 38.58−39.47).

Given the large number of different ore bodies used worldwide for nonferrous metal production in Europe (11, 46−48), it is impossible to constrain single ores as sources. As an approximation for early industrial Pb emissions (pre-1900), we used the isotopic composition from Pb−Zn ore deposits of Broken Hill (Australia). This Pb source made up the main share of nonferrous metal production from mid-19th century in England (49) and thus probably also in Switzerland as the trade routes of metal resources were similar within Europe (50). It is characterized by low radiogenic signatures (46) (^{206}Pb/^{207}Pb 1.03−1.10; ^{206}Pb/^{204}Pb 16.08−16.68).

Coal used for fuel combustion in Europe is derived mainly from Carboniferous and Triassic deposits in England, Germany, France, and Belgium (51), characterized by radiogenic Pb signatures (52, 53) (^{206}Pb/^{207}Pb 1.17−1.19; ^{206}Pb/^{204}Pb 18.29−18.57; ^{208}Pb/^{204}Pb 38.15−38.82).

Lead derived from open waste incineration is best represented by fly ash. We used data from waste incinerators of Switzerland, measured during the period 1975−1993 (54). The ratios were very constant during the whole period and more radiogenic than car exhausts (^{206}Pb/^{207}Pb ∼1.15; ^{206}Pb/^{204}Pb ∼17.95; ^{208}Pb/^{204}Pb ∼37.8) and in good agreement with fly ash from France and England (55). This range corresponds to the world average of the main Pb ore deposits and was used in other studies to represent recent industrial Pb (55).

To constrain the traffic source, we used Pb isotope ratios of car exhausts measured in Switzerland during 1993 (54) (^{206}Pb/^{207}Pb 1.08−1.14; ^{206}Pb/^{204}Pb 16.84−17.52; ^{208}Pb/^{204}Pb 36.57−37.24). Gasoline and thus car exhausts in Europe are nonradiogenic because Octel Co., the main producer of Pb-based antiknock compounds in fuels, uses Pb derived from Precambrian Pb−Zn ores in Australia, Morocco, and Canada (55).

Aerosols measured during the time period 1985−1994 were sampled in urban and rural environments in Switzerland (54). This Pb was similarly nonradiogenic as the traffic component (^{206}Pb/^{207}Pb 1.126−1.134; ^{206}Pb/^{204}Pb 17.51−17.68; ^{208}Pb/^{204}Pb 37.32−37.46).

It is important to keep in mind that the isotopic ratios of the contaminants may have been changing throughout the
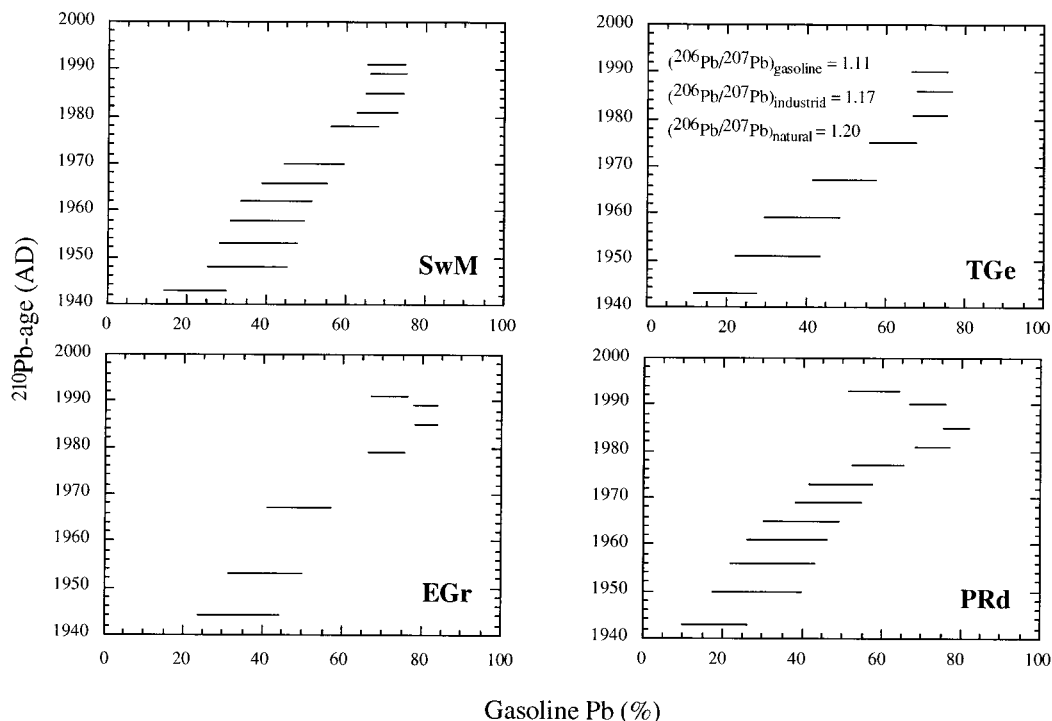
FIGURE 9. Calculated percentage contribution of gasoline-derived Pb to total airborne Pb in the peat bogs.

studied time period (*55*) and any characterization and assessment of possible sources is limited by this fact. To compensate for this uncertainty, the fields drawn in Figure 8 were enlarged slightly compared to the isotopic range given in the text.

Three Isotope Plots Involving ^{204}Pb, ^{206}Pb, *and* ^{207}Pb. Conventional three isotope diagrams are plotted with the ratios $^{206}Pb/^{204}Pb$ vs $^{207}Pb/^{204}Pb$ and $^{206}Pb/^{204}Pb$ vs $^{208}Pb/^{204}Pb$ for mathematical and geological correctness (*56*). Environmental scientists use diagrams incorporating $^{206}Pb/^{207}Pb$ ratios because of better analytical precision. Here we use $^{206}Pb/^{207}Pb$ vs $^{206}Pb/^{204}Pb$ diagrams for comparability with recent studies using ICP-MS and we also present conventional $^{206}Pb/^{204}Pb$ vs $^{207}Pb/^{204}Pb$ diagrams. In the present case, the $^{206}Pb/^{204}Pb$ vs $^{208}Pb/^{204}Pb$ diagrams (not shown) did not provide additional information compared to that given by the $^{206}Pb/^{207}Pb$ vs $^{206}Pb/^{204}Pb$ diagram.

Plotted on $^{206}Pb/^{207}Pb$ versus $^{206}Pb/^{204}Pb$, the ratios for all cores spread along a straight mixing line linking two possible end members: a nonradiogenic end member, represented by the traffic exhaust and Broken Hill Pb−Zn ores, and a radiogenic end member, represented by preanthropogenic aerosols and average upper continental crust (Figure 8). Major atmospheric contaminants such as urban aerosols, coal, or fly ash plot in between. The linear array defined in the diagram does not allow the source of pollution to be defined unequivocally. Until the late 19th and early 20th centuries, the isotopic compositions of the peats plot between the fields for coal and the natural, preanthropogenic aerosol and upper continental crust, implying coal as the main source of anthropogenic Pb at that time. Increasing As concentrations in the peat core at EGr (*1*) at that time supports this interpretation. Both As and Pb are often enriched in coals, relative to crustal abundance, and As is known to be often associated with Pb in coal ash (*57*). Since the turn of the century, the ratios became less radiogenic than coal, indicating that other sources such as e.g. Australian Pb from nonferrous metal production or fly ash from waste incineration became important in industrial emissions. Such early, nonradiogenic Pb has also been found in peat archives of Scotland (*2*) and herbage samples from England (*9*). The Pb

isotopes in peat samples at EGr and SwM (western and central Switzerland) pre-1967 plot between fly ash from waste incineration and preanthropogenic aerosols, and after that between fly ash and gasoline; this suggests that Pb from open waste incineration was an important source until roughly 1970, later giving way to traffic exhaust. This agrees well with emission inventories from Switzerland (*43*) and Europe (*58*). The isotopic composition of the peat samples from western and central Switzerland split into two populations with major gaps occurring between ca. 1979 and ca. 1967 at EGr and ca. 1975 and ca. 1967 at SwM, most likely due to the rapidly increasing leaded gasoline use (see also Figure 6). In southern Switzerland at GdL, all of the samples plot between the coal and fly ash field, implying that industrial Pb (represented by fly ash) is more important than traffic exhaust in this area.

When $^{207}Pb/^{204}Pb$ is plotted against $^{206}Pb/^{204}Pb$, the contaminants and peat bog samples become further separated. Although most of the data points are still linearly related within the measurement errors of the ratios (Figure 8), this presentation suggests that simple binary mixing between background and contaminant Pb is unlikely. The sites in central and western Switzerland in particular have some samples exhibiting lower $^{207}Pb/^{204}Pb$ ratios compared with GdL, possibly suggesting a third, industrially derived end member.

It is noteworthy that the isotopic ratios of aerosols measured in urban and rural Zürich between 1985 and 1994 (*54*) agree well with ratios from contemporary peats at EGr and SwM (Figure 8). Aerosol measurements made in Bern from 1965 to 1966 with $^{206}Pb/^{204}Pb$ ratios ranging from 17.88 to 17.65 (*11*) agreed also with contemporary peat samples: at EGr with 17.87 (1967), at PRd with 18.02 (1965), at TGe with 17.90 (1967), and at SwM with 17.98 (1966).

Contribution of Gasoline Lead to Total Lead Pollution after 1950. The isotopic composition of the peat bog samples after 1950 is unlikely to be explained by simple binary mixing between natural background aerosols and Pb derived only from waste incineration and coal (Figure 8). Traffic exhaust is an indisputable source given the emission inventories (*43*). Preanthropogenic aerosols, fly ash, or coal can be used as end members to reconstruct the observed signatures with

traffic exhaust (Figure 8). It is impossible to calculate the contribution of each component precisely, but the importance of traffic exhaust can be estimated graphically by binary mixing diagrams (54, 59) or using conventional mixing equations (55).

Here, binary mixing of gasoline and industrial Pb (represented by fly ash and coal taken together) was calculated using the following equation:

$$X_1 = [(^{206}Pb/^{207}Pb)_{sam} - (^{206}Pb/^{207}Pb)_{ind}]/$$
$$[(^{206}Pb/^{207}Pb)_{gas} - (^{206}Pb/^{207}Pb)_{ind}]$$

where X_1 represents the percentage contribution of gasoline Pb; $(^{206}Pb/^{207}Pb)_{gas}$, $(^{206}Pb/^{207}Pb)_{ind}$, and $(^{206}Pb/^{207}Pb)_{sam}$ are the isotopic signatures of the gasoline, the industrial end-members and of the peat bog samples, respectively.

Binary mixing between gasoline and the more radiogenic natural Pb component gives the following equation:

$$X_2 = [(^{206}Pb/^{207}Pb)_{sam} - (^{206}Pb/^{207}Pb)_{nat}]/$$
$$[(^{206}Pb/^{207}Pb)_{gas} - (^{206}Pb/^{207}Pb)_{nat}]$$

where X_2 represents the contribution of gasoline Pb and $(^{206}Pb/^{207}Pb)_{nat}$ is the natural, preanthropogenic isotopic composition. The range between X_1 and X_2 is a measure of the uncertainty on the estimate of the percentage contribution of gasoline-derived Pb when considering the mixing among gasoline Pb, industrial Pb, and natural Pb.

The average $^{206}Pb/^{207}Pb$ ratio of each end member used for the mixing calculations was 1.11 for gasoline, 1.17 for industrial (assuming a 1:1 mixture of coal and fly ash with average $^{206}Pb/^{207}Pb$ ratios of 1.19 and 1.15, respectively) and 1.20 for local, natural Pb. In Figure 9, the calculated contributions and uncertainties are shown for the cores TGe, PRd, EGr, and SwM. The core GdL was not considered due to its anomalous sources of industrial and gasoline Pb. Similar trends are found for all four cores: the proportion of gasoline Pb increases tremendously after the introduction of leaded gasoline and peaks between 70 and 80% in the late 1980s. The data suggests that although Pb emission from traffic have decreased largely during the last 10 years, the contribution from this source in modern peat is still detectable and seems to dominate the lead input from other sources. This interpretation agrees well with findings using recent snow samples in Switzerland (60).

Comparison with Other Archives of Atmospheric Pb Deposition. The observed changes of isotopic ratios against time using peat cores are consistent with other studies on atmospheric Pb deposition in Europe. Peat bog profiles from Scotland (2, 3) and Sweden (61), sediments from Switzerland (7) and Belgium (6), herbage samples from England (9), and time series measurements of aerosols from Western Europe (62) showed similar $^{206}Pb/^{207}Pb$ trends with decreasing ratios until the mid-1980s, and increasing later on due to the introduction of unleaded gasoline.

Implications for Pb Mobility and Peat Bog Archives. The consistent chronology of Pb isotopic composition and enrichment as found in the peats has two significant implications: (i) the atmospheric Pb input is quantitatively retained and becomes effectively immobile in the peat (1, 2, 16). The different isotope ratios between the two Pb-enrichment peaks show that the lower, older one is not a displacement of the upper, younger one; (ii) minerotrophic sites such as TGe and GdL can also be used to reconstruct the historical record of Pb deposition if atmospheric Pb dominates the total Pb budget.

Acknowledgments

Literature Cited

(1) Shotyk, W.; Cheburkin, A. K.; Appleby, P. G.; Fankhauser, A.; Kramers, J. D. *Earth Planet. Sci. Lett.* **1996**, *145*, E1−E7.
(2) MacKenzie, A. B.; Farmer, J. G.; Sugden, C. L. *Sci. Total Environ.* **1997**, *203*, 115−127.
(3) Farmer, J. G.; MacKenzie, A. B.; Sugden, C. L.; Edgar, P. J.; Eades, L. J. *Water, Air, Soil, Pollut.* **1997**, *100*, 253−270.
(4) Renberg, I.; Persson, M.; Emteryd, O. *Nature* **1994**, *368*, 323−326.
(5) Farmer, J. G.; Eades, L. J.; MacKenzie, A. B.; Kirika, A.; Bailey-Watts, T. E. *Environ. Sci. Technol.* **1996**, *30*, 3080−3083.
(6) Petit, D.; Mennessier, J. P.; Lamberts, L. *Atmos. Environ.* **1984**, *18*, 1189−1193.
(7) Moor, H.; Schaller, T.; Sturm, M. *Environ. Sci. Technol.* **1996**, *30*, 2928−2933.
(8) Jonsson, A.; Eklund, M.; Hakansson, K. *J. Environ. Qual.* **1997**, *26*, 1638−1643.
(9) Bacon, J. R.; Jones, K. C.; McGrath, S. P.; Johnston, A. E. *Environ. Sci. Technol.* **1996**, *30*, 2511−2518.
(10) Shotyk, W.; Weiss, D.; Appleby, P. G.; Cheburkin, A. K.; Frei, R.; Gloor, M.; Kramers, J. D.; Reese, S.; van der Knaap, W. O. *Science* **1998**, *281*, 1635−1640.
(11) Chow, T. J.; Snyder, C. B.; Earl, J. L. *Isotope ratios of lead as pollutant source indicators*, UN, FAO and IAEA Symposium, IAEA-SM-191/4; International Atomic Energy Agency: Vienna, 1975; pp 95−105.
(12) Birch, L.; Hanselmann, K. W.; Bachofen, R. *Water Res.* **1996**, *30*, 679−687.
(13) von Gunten, H. R.; Sturm, M.; Moser, R. N. *Environ. Sci. Technol.* **1997**, *31*, 2193-2197.
(14) Müller, K. Ph.D. Thesis, University of Bern, Switzerland, 1982.
(15) Norton, S. A.; Kahl, J. S. In *New approaches to monitoring aquatic ecosystems;* Boyle, T. P., Ed.; ASTM: Philadelphia, 1987; pp 40−57.
(16) Shotyk, W.; Appleby, P. G.; Cheburkin, A. K.; Fankhauser, A.; Kramers, J. D. *Water, Air, Soil Pollut.* **1997**, *100*, 297−310.
(17) Shotyk, W. *Water, Air, Soil Pollut.* **1996**, *84*, 1−31.
(18) Shotyk, W. *Environ. Rev.* **1996**, *4*, 149−183.
(19) Hill, B. M.; Siegel, D. I. *J. Hydrol.* **1991**, *123*, 211−224.
(20) Joray, M. *L'étang de la Gruère. Etude pollenanalytique et stratigraphique de la tourbière (L'étang de la Gruére. A pollen-analytical and stratigraphic study of the bog)*; Hans Huber Verlag: Bern, 1942; p 117.
(21) Welten, M. *Mitt. Naturforsch. Ges. Bern* **1964**, *21*, 67−73.
(22) Steinmann, P.; Shotyk, W. *Chem. Geol.* **1997**, *138*, 25−53.
(23) Steinmann, P.; Shotyk, W. *Geochim. Cosmochim. Acta* **1997**, *61*, 1143−1163.
(24) Mitchell, E. A. D. M.Sc. Thesis, University of Neuchâtel, Switzerland, 1995.
(25) Zoller, H.; Kleiber, H. *Verh. Naturforsch. Ges. Basel* **1971**, *81*, 90−154.
(26) Wardenaar, E. C. P. *Can. J. Bot.* **1987**, *65*, 1772−1773.
(27) Nriagu, J. O.; Lawson, G.; Wong, H. K. T.; Azcue, J. M. *J. Great Lakes Res.* **1993**, *19*, 175−182.
(28) Andrejko, M. J.; Fiene, F.; Cohen, A. D. In *Testing of peats and organic soils;* Jarret, P. M., Ed.; ASTM: Philadelphia, 1983; pp 5−20.
(29) Weiss, D.; Shotyk, W.; Cheburkin, A. K.; Gloor, M. *Analyst* **1998**, *123*, 2097−2102.
(30) Cheburkin, A. K.; Shotyk, W. *Fresenius J. Anal. Chem.* **1996**, *354*, 688−691.
(31) Hoffman, E. L. *J. Geochem. Explor.* **1992**, *44*, 297−319.
(32) Weiss, D.; Shotyk, W.; Schäfer, J.; Loyall, U.; Grollimund, E.; Gloor, M. *Fresenius J. Anal. Chem.* **1999**, *333*, 300−306.
(33) Appleby, P. G.; Nolan, P. J.; Gifford, D. W.; Godfrey, M. J.; Oldfield, F.; Anderson, N. J.; Battarbee, R. W. *Hydrobiology* **1986**, *143*, 21−27.
(34) Appleby, P. G.; Oldfield, F. In *Uranium Series Disequilibrium;* Ivanovich, M., Harmon, R. S., Eds.; Oxford University Press: Oxford, 1992; pp 731−778.
(35) Appleby, P. G.; Richardson, N.; Nolan, P. J. *Hydrobiology* **1991**, *214*, 35−42.

(36) Tolonen, K. *Bull. Geol. Soc. Finl.* **1984**, *56*, 207–219.

(37) Mörnsjö, T. *Bot. Not.* **1968**, *121*, 343–360.

(38) Anonymous. Technical report, Swiss Laboratory for Materials Testing and Research, Dubendorf, 1991.

(39) Weiss, D.; Shotyk, W.; Cheburkin, A. K.; Gloor, M.; Reese, S. *Water*, *Air*, *Soil Pollut.* **1997**, *100*, 311–324.

(40) Criqui, P. In *Physics and Chemistry of the Atmosphere of the Earth and other Objects of the Solar System;* Boutron, C. F., Ed.; Les Editions de Physique: Les Ulis, 1996; pp 277–297.

(41) Pacyna, J. M.; Scholtz, T. M.; Li, Y.-F. *Environ. Rev.* **1995**, *3*, 145–159.

(42) Settle, D. M.; Patterson, C. C. *Science* **1980**, *207*, 1167–1176.

(43) BUWAL. *Vom Menschen verursachte Luftschadstoffe-Emissionen in der Schweiz von 1900 bis 2010 (Emissions of pollutants from human activities in Switzerland from 1900 to 2010)*; Bundesamt für Umwelt, Wald und Landschaft: Bern, Switzerland, 1995; p 121.

(44) Döring, T. Ph.D. Thesis, University of Bern, Switzerland, 1997.

(45) Kramers, J. D.; Tolstikhin, I. N. *Chem. Geol.* **1997**, *139*, 75–110.

(46) Doe, R. B. *Lead Isotopes*; Springer-Verlag: Berlin, 1970; p 137.

(47) Hopper, J. F.; Ross, H. B.; Sturges, W. T.; Barrie, L. A. *Tellus* **1991**, *43B*, 45–60.

(48) Sturges, W. T.; Barrie, L. A. *Atmos. Environ.* **1989**, *23*, 132–139.

(49) Day, J.; Tylecote, R. F. *The Industrial Revolution in Metals*; The Institute of Metals: London, 1991; p 213.

(50) Anonymous. *Schweizerische Handelstatistik, Jahresbericht 1935 (Swiss Trade Statistics, Annual Report 1935)*; Eidgenössische Oberzolldirektion: Bern, 1935; Parts 1 and 2, p 413.

(51) Grossling, B. *World Coal Resources*; The Financial Times Ltd: London, 1979; p 153.

(52) Walraven, N.; van Os, B. J. H.; Klaver, G. T.; Baker, J. H.; Vriend, S. P. *J. Geochem. Explor.* **1997**, *59*, 47–58.

(53) Sugden, C. L.; Farmer, J. G.; MacKenzie, A. B. *Environ. Geochem. Health* **1993**, *15*, 59–65.

(54) Hansmann, W.; Köppel, V.; Saager, R.; Steiger, R. *Chem. Geol.* **1999**, in preparation.

(55) Monna, F.; Lancelot, J.; Croudace, I. W.; Clundy, A. B.; Lewis, J. T. *Environ. Sci. Technol.* **1997**, *31*, 2277–2286.

(56) Köppel, V.; Grünenfelder, M. In *Lectures in Isotope Geology;* Jäger, E., Hunziker, J. C., Eds.; Springer-Verlag: Heidelberg, 1979; pp 135–153.

(57) Vijayan, V.; Behera, S. N.; Ramamurthy, V. S.; Puri, S.; Shahi, J. S.; Singh, N. *X-ray Spectrom.* **1997**, *26*, 65–68.

(58) Olendrzynski, K.; Anderberg, S.; Bartnicki, J.; Pacyna, J. M.; Stigliani, W. *Environ. Rev.* **1996**, *4*, 300–320.

(59) Faure, G. *Principles of Isotope Geology*; John Wiley and Sons: London, 1986; p 453.

(60) Döring, T.; Schwikowski, M.; Gäggeler, H. W. *Fresenius J. Anal. Chem.* **1997**, *359*, 382–384.

(61) Bränvall, M. L.; Bindler, R.; Emteryd, O.; Nilsson, M.; Renberg, I. *Water*, *Air*, *Soil*, *Pollut.* **1997**, *100*, 243–252.

(62) Grousset, F. E.; Quétel, C. R.; Thomas, B.; Buat-Ménard, P.; Donard, O. F. X.; Bucher, A. *Environ. Sci. Technol.* **1994**, *28*, 1605–1608.